Dynamic response characteristics of thermoelectric generator predicted by a three-dimensional heat-electricity coupled model

Jing-Hui Meng [a], Xin-Xin Zhang [a], Xiao-Dong Wang [b,c,*]

[a] School of Mechanical Engineering, University of Science and Technology Beijing, Beijing 100083, China
[b] State Key Laboratory of Alternate Electrical Power System with Renewable Energy Sources, North China Electric Power University, Beijing 102206, China
[c] Beijing Key Laboratory of Multiphase Flow and Heat Transfer for Low Grade Energy, North China Electric Power University, Beijing 102206, China

HIGHLIGHTS

• A transient TEG model was proposed with consideration of heat-electricity coupling.
• The dynamic characteristics of the TEG was studied numerically.
• Four kinds of variations in application environments were designed.
• Response hysteresis of power and overshoot/undershoot of efficiency were found.

ARTICLE INFO

ABSTRACT

The practical application environments of thermoelectric generators (TEGs) always change, which make a requirement for studying the dynamic response characteristics of TEGs. This work develops a complete, three-dimensional and transient model to investigate this issue. The model couples the energy and electric potential equations. Seebeck effect, Peltier effect, Thomson effect, Joule heating and Fourier heat conduction are taken into account in this model. Dynamic output power and conversion efficiency of the TEG, which are caused by variations of the hot end temperature, cold end temperature and load current, are studied. The response hysteresis of the output power to the hot end and cold end temperatures, the overshoot or undershoot of the conversion efficiency are found and attributed to the delay of thermal diffusion. However, the output power is synchronous with the load current due to much faster electric response than thermal response.

© 2013 Elsevier B.V. All rights reserved.

1. Introduction

Alternative green energy technology which aims to reduce greenhouse gas emissions and fossil fuel usage has become one of the most popular researches in the background of the current energy crisis. As one of the alternatives, thermoelectric technology has attracted great attention in the last decade due to its excellent features, such as no mechanical moving parts, no refrigerants, layout flexibility, low maintenance costs, long run-time and other advantages [1–3]. Thermoelectric devices, which consist of tens to hundreds of pairs of p-type and n-type semiconductors, can be divided into two different groups: thermoelectric cooler (TEC) [4–6], which directly convert electricity to thermal energy for cooling purpose based on the Peltier effect, and thermoelectric generator (TEG) [7–9], driven by large temperature differences to convert the heat into electrical power based on the Seebeck effect.

The TEG performance, including the output power and conversion efficiency, is not only related to the properties of thermoelectric materials, but also closely related to the operating conditions. For a long time, the TEG conversion efficiency had been very low due to limitation of thermoelectric materials, hence, the TEG technology was only used in aerospace and other cutting-edge areas [10]. However, with the successful development of new thermoelectric materials and the significant improvement of the TEG conversion efficiency, the TEG technology has been regarded as a promising power generator in civilian applications, thus, a number of works have been carried out to investigate the characteristics of the TEG [11–20].

Almost all of the existing literature of TEGs carried out the performance evaluation in steady-state conditions [7–9,11–20],

* Corresponding author. State Key Laboratory of Alternate Electrical Power System with Renewable Energy Sources, North China Electric Power University, Beijing 102206, China. Tel./fax: +86 10 6232 1277.
E-mail address: wangxd99@gmail.com (X.-D. Wang).

the transient performance was concerned only in a few literature [21–23]. In fact, the practical application environments of TEGs always change. First of all, the heat source temperature will change with varied supplies, for example, the coal or fuel supply rate can not be static in iron and steel works, power generating and chemical industries, leading to time-dependent industrial waste heat; for the collection of automobile exhaust heat, the amount of heat will increase with the acceleration and reduce with the deceleration of the automobile. Secondly, the consumption demand for electrical energy inevitably varies in different time scale, which makes a requirement for the change of load current in the TEG system. Thirdly, the temperature of the cold end of the TEG will be changed with the flow rate of cooling medium in heat sinks. Furthermore, the thermoelectric transient behavior is particularly apparent in the start-up and shut-down stages of the devices. Once the above-mentioned changes occur, the output power and conversion efficiency of the TEG will change, showing the dynamic behavior, the original steady-state equilibrium is destroyed, while the formation of a new steady-state will inevitably consume a certain time.

Chen et al. [21] studied the transient behavior of the TEG when the user load was changed based on the energy balance equations only at the hot and cold ends (zero-dimensional model), the model divided both the Joule heat and the Thomson heat into two equal parts, one part flows to the hot end, and the other to the cold end of the TEG, however, it is not strictly accurate, because the Joule heat and Thomson heat are the inner heat sources. Moreover, this method does not solve the internal temperature distribution of the TEG, so that dependence of TEG performance on the internal heat transfer and carrier transport can not be understood well. Montecucco et al. [22] used the method of solving one-dimensional heat conduction equation to study the transient characteristics of the TEG when the load was changed, but ignored the three-dimensional effect of the TEG. Alata et al. [23] also developed a one-dimensional transient TEG model to investigate the dynamic variation of conversion efficiency with increased load current. Compared with Montecucco et al.'s model, the Thomson effect was taken into account in Ref. [23]. In these models [21–23], the current density, J, was assumed to be distributed uniformly within the whole TEG, so that $J = I/A$, where I is the load current and A is the cross-sectional area of semiconductors. However, our previous [24,25] and Cheng's [26] works have shown that there exists coupling of temperature field and electric potential field within semiconductors for the TEC, which causes three-dimensional temperature and current distributions, especially for high temperature differences and large applied currents. Thus, it is expected that this coupled effect may also be important for the TEG, because the TEG generally operates in larger temperature differences than the TEC in order to produce a higher output power. Furthermore, these studies [21–23] focused on the dynamic characteristics only when the load current was changed, in practice, transient operating conditions of the TEG are caused by variation of not only the load current, but also temperatures of the hot or cold ends. Thus, understanding the dynamic characteristics of the TEG induced by variations of hot or cold heat sources is necessary for the design and operation of the TEG.

The objective of this work is to develop a fully three-dimensional and transient TEG model, which introduces the coupling of heat transfer and electric conduction within semiconductors. The model is adopted to investigate the transient characteristics of the TEG. Four kinds of variation patterns (i.e. step increase, linear increase, step decrease and linear decrease) in the hot end temperature, the cold end temperature and the load current are respectively designed to reveal the dynamic output power and conversion efficiency of the TEG, which can provide some useful insight into response mechanism for practical TEG applications.

2. Model

A TEG device in essence is a thermopile composed of a number of p- and n-type semiconductor pairs. Because the thermal characteristics are the same for all TEG elements, only one element is considered here. Fig. 1 shows the schematic of the TEG element, it includes a columnar p-type semiconductor and a columnar n-type semiconductor which are sandwiched between copper connectors, there are two ceramic plates at both ends of the connectors for insulation. The thicknesses of the ceramic plate, metal connector and semiconductor are H_0, H_1 and H_2, respectively, the cross-sectional areas of p- and n-type semiconductors are same and equal to $L_2 \times L_2$ with a separation distance of L_1.

Charge carriers in p- and n-type semiconductor are holes and electrons, respectively. When the TEG element is sandwiched between the hot and cold sources, the hot end of the TEG absorbs heat from the hot source and the cold end releases heat to the cold source due to carriers transport, which causes conversion of thermal energy into electrical energy in the form of electromotive force or output current.

2.1. Governing equations

The three-dimensional transient TEG model established in this paper includes the energy equation and the electric potential equation. The energy equations of the metal connector, the p-type semiconductor, the n-type semiconductor, and the ceramic plate are as follow:

$$(\rho c_p)_i \frac{\partial T}{\partial t} = \nabla \cdot (\lambda_i \nabla T) + \frac{J^2}{\sigma_i} - \beta_i \overrightarrow{J} \cdot \nabla T \tag{1}$$

where, ρ is the density, c_p is the specific heat, λ is the thermal conductivity, σ is the electric conductivity, and β is the Thomson coefficient. The subscript i is conn for connectors, p for the p-type semiconductor, n for the n-type semiconductor, cer for ceramic plates, respectively. The first term on the right side in Eq. (1) denotes the Fourier heat conduction, the second and third terms denote the internal heat sources due to the Joule heating and Thomson effect. $J(x, y, z)$ is the local current density, and $J = 0$ for the ceramic plate. The Thomson coefficient is proportional to the first derivative of the Seebeck coefficient versus temperature, or:

$$\beta = T \frac{d\alpha}{dT} \tag{2}$$

where, α is the Seebeck coefficient of semiconductors.

The driving force for carriers is the electric potential, which can be expressed as follows:

$$\nabla \cdot \left(\sigma(\nabla \phi - \alpha \nabla T) + \varepsilon \nabla \frac{\partial \phi}{\partial t} \right) = 0 \tag{3}$$

where, ϕ is the electric potential, $\alpha \nabla T$ is the Seebeck electromotive force coming from the Seebeck effect, ε is the permittivity.

The electric field can be calculated by the following equation:

$$\overrightarrow{E} = -\nabla \phi + \alpha \nabla T \tag{4}$$

Thus, the current density in Eq. (1) can be calculated as follows:

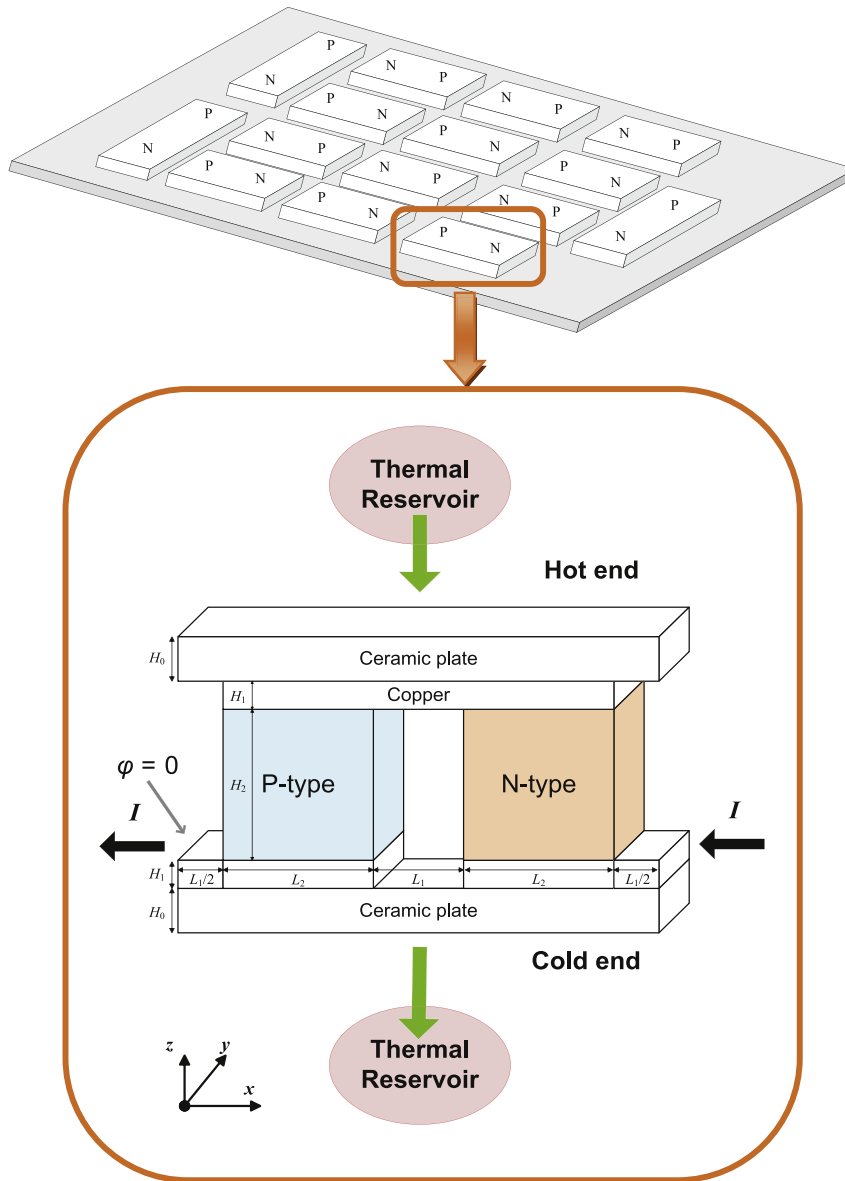$$\overrightarrow{J} = \sigma \overrightarrow{E} \tag{5}$$

Fig. 1. The schematic of TEG element.

Generally, the performance of the TEG is evaluated by two parameters: output power, P, and conversion efficiency, η, which are defined as follows:

$$P = IV \qquad (6)$$

$$\eta = \frac{P}{Q_h} \qquad (7)$$

where, I is the load current, V is the output voltage, Q_h is the heat supplied to the hot end of the TEG.

2.2. Initial and boundary conditions

The purpose of this paper is to study the dynamic characteristics of the TEG when the application environments are changed, including hot end temperature, cold end temperature and load current. The boundary conditions of the model are set as follows.

For a practical operation, the TEG absorbs heat from a hot source such as industrial flue gas or automobile exhaust gas, and the heat is dissipated by a heat sink (cold source). Thus, the third kind boundary condition should be used if the hot and cold sources are not included in the modeling. However, for simplified purpose, the hot and cold sources are assumed to be infinite constant heat reservoirs in the present model, hence, the third kind boundary condition is substituted by the first kind one. In addition, our preliminary tests showed that there is no qualitative difference for dynamic response characteristics of the TEG although quantitative difference exists when this simplification is adopted. Adiabatic boundary conditions are applied to the outside surfaces of the TEG with continuity assumption for temperature and heat flux on the interfaces between different materials.

For the electric boundary conditions of the TEG, assumptions of constant current and zero electric potential are adopted for the inlet and the outlet, respectively, as shown in Fig. 1. There is no current flowing out on the other surfaces, thus, $\vec{J} \cdot \vec{n} = 0$. Besides, initial temperature of the TEG element is equal to the

Table 1
Properties of the materials used in the present work [28].

Materials	k (W K^{-1} m^{-1})	$1/\sigma$ (S m^{-1})	α (V K^{-1})
n-type (Bi$_2$Te$_3$)	1.6	7.69×10^4	-2.28×10^{-4}
p-type (Sb$_2$Te$_3$)	2.1	9.62×10^4	1.71×10^{-4}
Connector (Cu)	350	5.90×10^8	–
Ceramic plate (Si)	130	–	–

environmental temperature $T_\infty = 300$ K, and initial electric potential is zero.

3. Simulation cases

The geometry of the TEG adopted for simulations has $H_0 = 0.9$ mm, $H_1 = 0.2$ mm, $H_2 = 1.9$ mm, $L_1 = 0.5$ mm, and $L_2 = 1.0$ mm. Sb$_2$Te$_3$ and Bi$_2$Te$_3$ are chosen for the p-type and n-type semiconductors due to their excellent thermoelectric properties from room temperature to 500 K [27]. The connector and ceramic plate are made of copper and Si, respectively. All of the material properties are listed in Table 1.

The transient behaviors of the TEG are mainly triggered by changes of the working environment and consumer's consumption demand for electric power. For comparison purpose, a base-line case with hot end temperature $T_h = 450$ K, cold end temperature $T_c = 300$ K, and load current $I = 0.5$ A is chosen and analyzed firstly. The step increase or decrease and the linear increase or decrease is designed to simulate the changes of T_h, T_c and I, respectively. Thus, twelve cases are simulated as listed in Table 2, in which only one parameter is changed for each case with the other two parameters as the same as the base-line case.

4. Model validation

Due to the lack of experimental data of the transient response performance of the TEG in the open literature, the model is validated only for the steady-state operation. Q_h, I, P, and η, were compared with one-dimensional steady-state analytical solution of Angrist et al. [29] and numerical prediction of Chen et al. [8]. In the analytical solution, the thermal conductivity, electric conductivity, and Seebeck coefficient of semiconductors were all assumed to be temperature-independent, and adiabatic boundary conditions were assumed on the side surfaces of TEG element. Our simulation is performed for a TEG device with 127 elements, each element has the geometry of $H_1 = 0.2$ mm, $H_2 = 1.6$ mm, $L_1 = 0.5$ mm, and $L_2 = 1.4$ mm, as well as constant material properties of $\alpha_p = -\alpha_n = 226.8 \times 10^{-6}$ V K^{-1}, $k_p = k_n = 1.52$ W m^{-1} K^{-1} and

Table 2
Cases simulated in the present work.

Case	Parameters	Value before changing	Variational form	Value after changing	Unit
1	T_h	450		500	K
2	T_c	300	⌐	320	K
3	I	0.5		0.7	A
4	T_h	450		500	K
5	T_c	300	╱	320	K
6	I	0.5		0.7	A
7	T_h	450		400	K
8	T_c	300	⌐_	280	K
9	I	0.5		0.3	A
10	T_h	450		400	K
11	T_c	300	╲	280	K
12	I	0.5		0.3	A

$\sigma_p = \sigma_n = 1.447 \times 10^{-5} \Omega$ m. In addition, the heat loss to the ambient is ignored for comparison with the theoretical solution. The same geometry and material properties were also used in Chen et al.'s simulation [8].

The simulation was conducted for three sets of grid systems (coarse grid, medium grid, and refined grid). The present and Chen et al.'s [8] numerical predictions and the theoretical evaluation [29] for Q_h, I, P, and η are shown in Table 3. Present prediction has better agreement with the theoretical evaluation than Chen et al.'s. The maximum deviation between the present prediction with the coarse grid and the theoretical evaluation is 3.5%, 2.5% for the medium grid, and 2.0% for the refined grid. Restated that the theoretical solution [29] was driven based on the assumptions of steady-state operation, one-dimensional temperature distribution, uniform current density, constant material properties, and no heat loss to the ambient, therefore, its applicability will be limited when the operating condition of the TEG deviates from these assumptions. However, the present model is more general with three-dimensional distributions of temperature and current density, which can be used to study the transient or steady performance of the TEG at more complicated operating conditions such as high temperature difference and/or large heat loss to the ambient.

The grid independence for the TEG geometry used in the case studies was examined in preliminary test runs. The independence of the time step size, Δt, was also examined as shown in Fig. 2 with Δt then taken as 0.001 s.

5. Results and discussion

5.1. The effect of hot end temperature

5.1.1. Step and linear decreases

Fig. 3 shows variations of P with time for the step and linear decreases in T_h. For the step variation, T_h decreases sharply from 450 K to 400 K at 0.01 s, however, P does not change synchronously which reaches the new steady-state value of 0.0083 W at $t = 0.052$ s. For the linear variation, T_h decreases from 450 K at $t = 0.01$ s to 400 K at $t = 0.06$ s with reduction rate of 1 K m s^{-1}, and the new steady state is observed at $t = 0.086$ s with the same P value of 0.0083 W. The results indicate that there exists a temporal hysteresis in the response of P to T_h. The hysteresis is attributed to the delay of thermal diffusion from the ceramic plate to the hot junction. The response time is defined as the time required to reach a new steady state after the outside environment (T_h, T_c or I) stops changing. The response time of P is 0.042 s (=0.052 s − 0.01 s) for the step decrease and 0.026 s (=0.086 s − 0.06 s) for the linear decrease, which indicates that the response time shortens once the reduction rate of T_h is reduced.

Fig. 4 shows the dynamic variations of Q_h for the step and linear decreases in T_h. For the step variation, T_h decreases from 450 K to 400 K at $t = 0.01$ s, which causes a sharp reduction in Q_h from 0.3721 W to −68.4293 W at $t = 0.011$ s, then Q_h gradually increases and again reaches zero at $t = 0.051$ s, finally, the new steady state

Table 3
Comparisons of numerical predictions and analytical solutions ($T_h = 423$ K and $T_c = 303$ K).

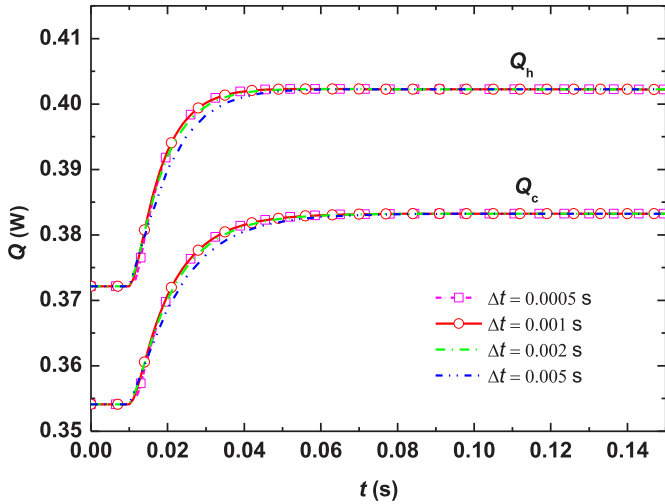| Quantity	Analytical results [29]	Chen et al.'s results [8]	Grid system1 (75081 grids)	Grid system2 (241101 grids)	Grid system3 (557289 grids)
Q_h (W)	81.3	81.8	81.2	81.2	81.2
P (W)	3.98	3.62	3.84	3.88	3.90
I (A)	1.08	1.032	1.08	1.08	1.08
η	4.89	4.43	4.73	4.77	4.80

Fig. 2. Dynamic variations of Q_h and Q_c with various time step lengths for increased load current.

corresponding to $T_h = 400$ K is reconstructed at $t = 0.095$ s. For the linear variation, Q_h firstly decreases from the initial value of 0.3721 W to the minimum value of -5.8711 W ($Q_{h,min}$) at $t = 0.06$ s, then increases to zero at $t = 0.085$ s and finally reaches the steady state at $t = 0.127$ s. It is noted that a negative value of Q_h occurs during 0.01–0.052 s for the step variation and 0.01–0.085 s for the linear variation, which means that the hot end of the TEG does not absorb but liberate the heat to the ambient, however, the TEG still generates electricity. This abnormal phenomenon can be explained by the internal temperature distribution of the TEG as shown in Fig. 5.

Fig. 5 shows the temperature distributions along the TEG height direction at $x = 0.75$ mm and at different times for the step and linear decreases in T_h. For the step variation, T_h is 450 K and the temperature at the top of p-type semiconductor, $T_{p,top}$, is 448.0 K at $t = 0.01$ s, with only 2 K temperature difference due to high thermal conductivities of the ceramic plate and metal connector. At $t = 0.011$ s, T_h decreases sharply to 400 K, however, $T_{p,top}$ is only decreases to 443.6 K due to the delay of the thermal diffusion from the ceramic plate to the hot junction. $T_{p,top}$ gradually decreases at 0.011 s $< t <$ 0.052 s, however, it always higher than T_h, thus, a positive temperature gradient from the hot junction to the ceramic plate is formed, which causes a heat release of the TEG to the ambient. The maximum temperature gradient occurs at $t = 0.011$ s
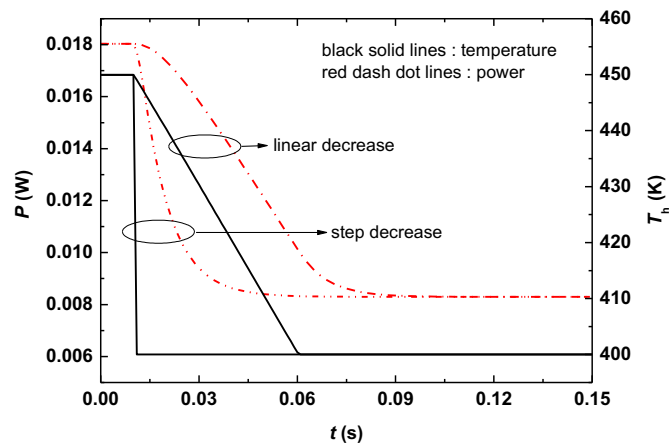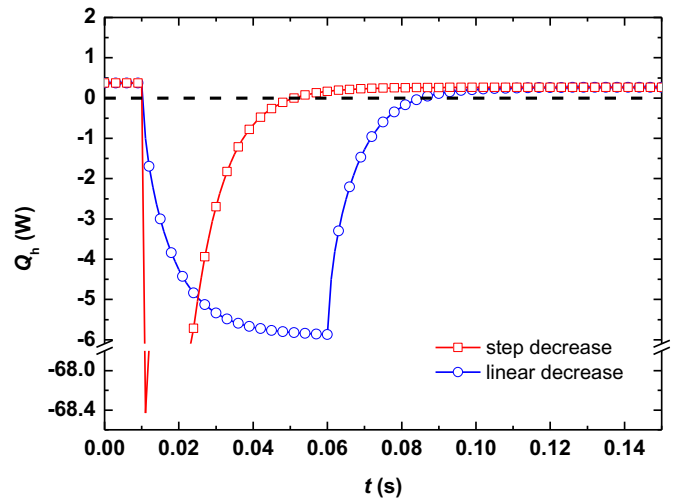

Fig. 4. Dynamic variations of Q_h for the linear and step decreases in T_h.

for the step variation, so that the maximum heat release is observed at the same moment (Fig. 4). At $t = 0.052$ s, $T_{p,top}$ decreases to 399.2 K, which is lower than T_h, and hence the TEG starts to absorb the heat from the ambient again. P is mainly determined by
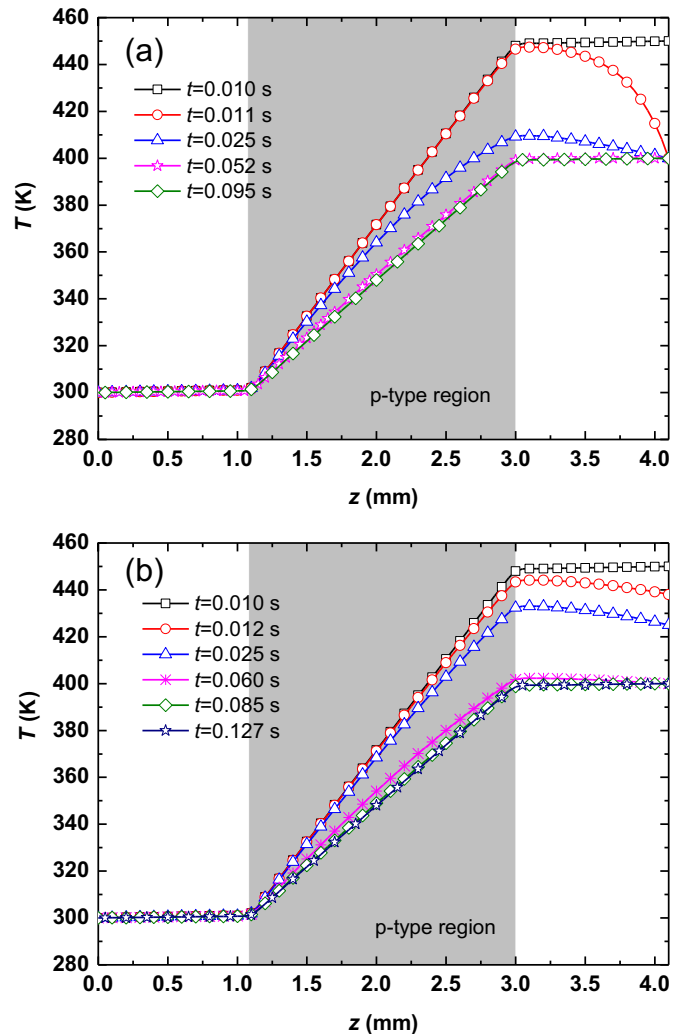

Fig. 5. The temperature distributions along the TEG height direction at different times: (a) step decrease; (b) linear decrease.

Fig. 3. Dynamic output power variations for the linear and step decreases in T_h.

temperature distribution of p-type and n-type semiconductors. Fig. 5a shows that the temperature at the bottom of the p-type semiconductor, $T_{p,bottom}$, is almost kept at 300 K, while $T_{p,top}$ continuously decreases from 448.0 K ($t = 0.01$ s) to 398.6 K ($t = 0.095$ s) throughout the whole transient process, which causes a continuous reduction in the temperature difference between $T_{p,bottom}$ and $T_{p,top}$ and hence a continuous reduction in P of the TEG (Fig. 3). For the linear variation, T_h decreases from 450 K to 400 K with a finite reduction rate of 1 K m s^{-1}, the response of $T_{p,top}$ is slower than the step variation. For example, $T_{p,top}$ decreases to 409.3 K at $t = 0.025$ s for the step variation (Fig. 5a), however, it only decreases to 432.4 K for the linear variation (Fig. 5b). The slower response of $T_{p,top}$ is the reason why the times, at which $Q_{h,min}$, $Q_h = 0$ and the new steady state are reached, are delayed for the linear variation as compared to the step variation.

The dynamic variations of η for the step and linear decreases in T_h are shown in Fig. 6. According to Eq. (7), η is defined as the ratio of P to Q_h. At $t \leq 0.01$ s, the TEG operates at steady state with $T_h = 450$ K and $T_c = 300$ K, and η is 4.85%. At 0.01 s < t < 0.051 s for the step variation and at 0.01 s < t < 0.085 s for the linear variation, the TEG liberates the heat to the ambient, which implies that the output power is generated without the outside heat input, so that an infinite η occurs. At $t = 0.052$ s for the step variation and at $t = 0.086$ s for the linear variation, the TEG starts to absorb the heat from the ambient again, thus, a finite $\eta = 31.69\%$ for the step variation and $\eta = 39.72\%$ for the linear variation occurs, then η decreases due to the reduced temperature difference ($=T_{p,top} - T_{p,bottom}$) and P until the TEG reaches the new steady state with $\eta = 3.12\%$.

5.1.2. Step and linear increases

Dynamic variations of the P and η for the step and linear increases in T_h are shown in Fig. 7. For the step variation, T_h increases sharply from 450 K to 500 K at $t > 0.01$ s, however, for the linear variation, T_h increases from 450 K to 500 K at 0.01 s < t < 0.06 s with an increase rate of 1 K m s^{-1}. Because the increase in T_h elevates the temperature difference between the hot and cold junctions, $T_{p,top} - T_{p,bottom}$ ($\approx T_{n,top} - T_{n,bottom}$), and the temperature difference becomes larger and larger with the time increased, P gradually rises until the TEG reaches the new steady state. The temporal hysteresis in the response of P to T_h is also observed for the present two cases due to the delay of the thermal diffusion from the ceramic plate to the hot junction.
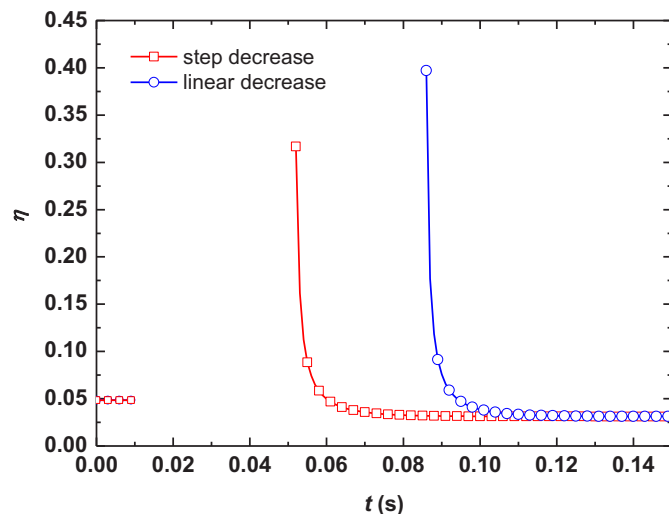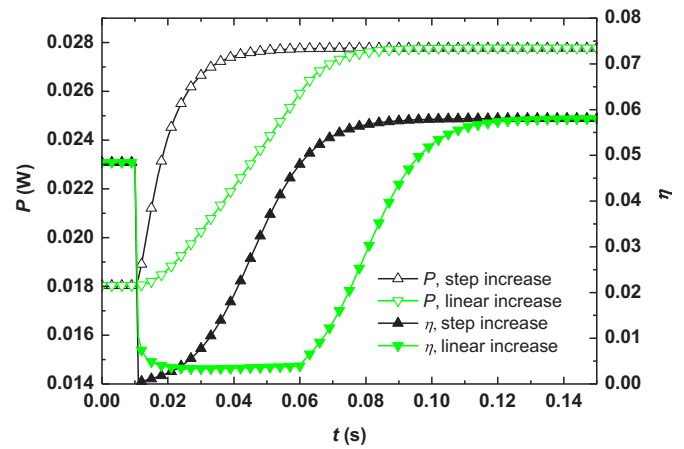

Fig. 7. Dynamic variations of the power and conversion efficiency for the step and linear increases in T_h.

Fig. 7 also shows that there exists an undershoot of η for both step and linear increases despite the continuously increased P. The undershoot occurs at 0.01 s < t < 0.011 s for the step increase and at 0.01 s < t < 0.06 s for the linear increase. The undershoot is more intense for the step increase, η almost reduces to zero at $t = 0.011$ s, which is much lower than its initial value of 0.0180 W. This phenomenon can be attributed to the lag of $T_{p,top}$ ($\approx T_{n,top}$) variation behind T_h due to finite thermal diffusion rate from the ceramic plate to the hot junction of the TEG.

5.2. The effect of cold end temperature

Step and linear variations in T_c are designed, respectively, to analyze the effect of T_c on the dynamic characteristics of the TEG. The TEG operates at steady state with $T_h = 450$ K and $T_c = 300$ K at $t \leq 0.01$ s, then T_c starts to increase or decrease from 300 K with $\Delta T = 20$ K at $t > 0.01$ s. For the linear variation, the increase or decrease rate of T_c is taken as 0.4 K m s^{-1}. Fig. 8 shows that the power curves for the increase and decrease cases have symmetry. For example, P is increased from its initial value of 0.0180 W— 0.0219 W with $\Delta P = 0.039$ W at 0.038 s for the step decrease, while is decreased to 0.0141 W with the same $\Delta P = 0.039$ W at the same time for the step increase. Reduction of P due to increasing T_c can be attributed to reduced temperature difference between the hot and
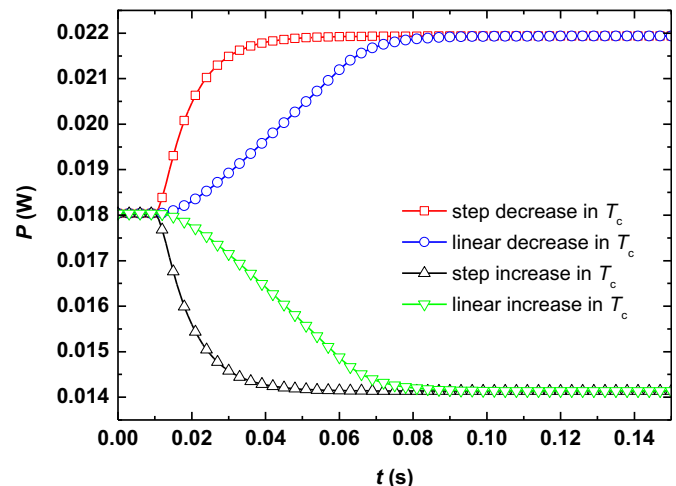

Fig. 6. Dynamic variations of conversion efficiency for the step and linear decreases in T_h.

Fig. 8. Dynamic variations of the output power for the decrease and increase in T_c.
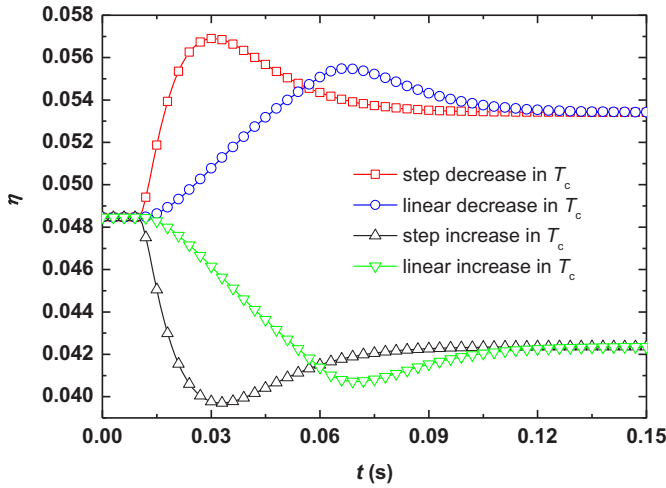
Fig. 9. Dynamic variations of the conversion efficiency for the decrease and increase in T_c.

Fig. 11. Dynamic variations of output power for the step and linear variations in I.

cold ends of the TEG, and vice versa. The hysteresis of response of P to T_c is once again observed for all the four cold temperature variations. The TEG reaches the new steady state at 0.038 s with the response time of 0.028 s for the two step variations, while the response time shortens to 0.013 s ($=0.073 - 0.06$) for the two linear variations.

Dynamic variations of η for the step and linear variations in T_c is shown in Fig. 9. Note that overshoot of η is observed for the step and linear decreases in T_c, while undershoot for the step and linear increases. Due to the delay of thermal diffusion, T_h has the slowest response to T_c, and then followed by $T_{p,top}$ ($\approx T_{n,top}$) and $T_{p,bottom}$ ($\approx T_{n,bottom}$). Thus, for the decrease cases in T_c, the increase rate of Q_h is lower than P, which causes the overshoot of η. The response of $T_{p,bottom}$ ($\approx T_{n,bottom}$) for the step decrease is faster and stronger than that for the linear decrease, and hence the overshoot of η occurs earlier with the higher peak value. The similar reason can be used to explain the undershoot of η for the increase cases in T_c.

5.3. The effect of load current

The simulations are performed with fixed $T_h = 450$ K and $T_c = 300$ K. The initial load current, I, is 0.5 A at $t \le 0.01$ s, it varies to 0.7 A at $t > 0.01$ s for the step and linear increases, and to 0.3 A for
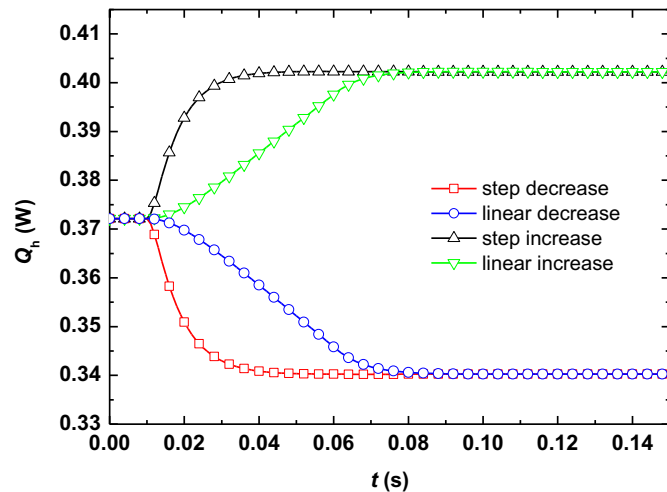
the step and linear decreases. The increase or decrease rate of I is 4 A s^{-1} for the linear cases. The dynamic responses of Q_h for the step and linear variations in I are shown in Fig. 10. The steady state is reached at 0.039 s for the step increase, at 0.043 s for the step decrease, at 0.075 s for the linear increase, and at 0.080 s for the linear decrease. These results indicate that Q_h lags behind I. The lag behavior can be explained as follow. Because Joule heat and Thomson heat are volumetric heat sources and are proportional to I^2 and I, although the internal heat sources response immediately when I is varied, the temperature distribution can not response synchronously due to the finite thermal diffusion rate.

Dynamic variations of P for the step and linear cases are shown in Fig. 11. The response of P is almost synchronous with I, which indicates that the electric response of the TEG is much faster than the thermal response. The steady-state I–P curve with fixed $T_h = 450$ K and $T_c = 300$ K is shown in Fig. 12. If the P–t curve (0.01 s $\le t \le 0.06$ s) in Fig. 11 is converted into the I–P curve, the I–P curve almost coincide to the steady-state one in the same range of load current (0.5 A $\le I \le 0.7$ A) as shown in Fig. 12, which further confirms that the electric response time of the TEG can be almost neglected. Dynamic variations of conversion efficiency for the step and linear variations in I are shown in Fig. 13. Temporal hysteresis in the response of η to I for the four cases, overshoot for the two

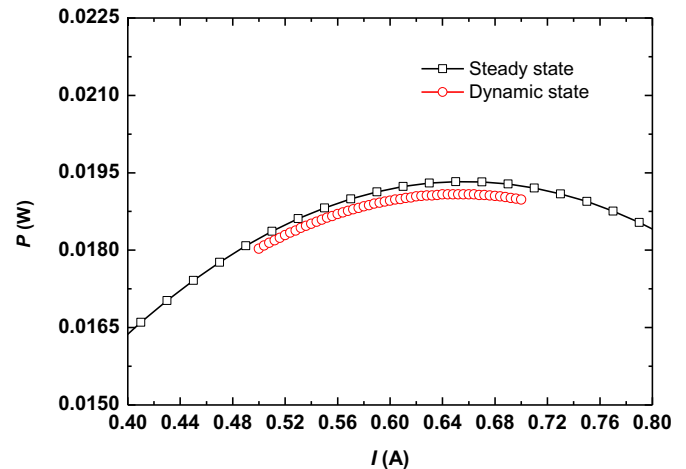**Fig. 10.** The dynamic variation of Q_h for the step and increase variation in I.

Fig. 12. Comparison between the steady-state and dynamic I–P curves with fixed $T_h = 450$ K and $T_c = 300$ K.
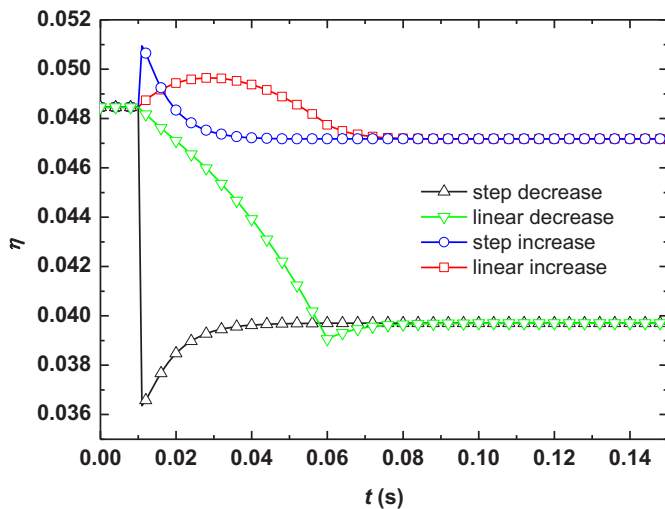
Fig. 13. Dynamic variations of conversion efficiency for the step and linear variations in I.

increase cases, and undershoot for the two decrease cases are observed, respectively. These phenomena can be attributed to the synchronous variation of P and the lagging of Q_h when I is varied.

6. Conclusions

This paper developed a complete, three-dimensional and transient TEG model, the model solved the temperature and electric potential equations and accounted for all thermoelectric effects. The model was used to investigate the dynamic characteristics of the TEG when the application environments are changed. Thermoelectric materials Bi_2Te_3 and Sb_2Te_3 were selected as n-type and p-type semiconductors. Four kinds of typical cases, the step increase and decrease and the linear increase and decrease in the hot end temperature, the cold end temperature, and the load current, were designed to investigate their effects on the dynamic characteristics of the TEG. The main conclusions are as follows:

1) For the variation of the hot end temperature, increasing the hot end temperature elevates the output power and the heat amount adsorbed from the ambient, however, the growth rate of the heat amount is higher than that of the output power, which causes an undershoot of the conversion efficiency. Decreasing the hot end temperature reduces the output power and produces a positive temperature gradient from the hot junction to the ceramic plate, which causes a heat release of the TEG to the ambient and infinite conversion efficiency. The temporal hysteresis in the response of the output power to the hot end temperature is observed for all the four cases due to the delay of the thermal diffusion from the ceramic plate to the hot junction.

2) When the cold end temperature is varied, increasing the cold end temperature reduces the output power, and vice versa. The response hysteresis of the output power to the cold end temperature is observed and the response time for the linear variation is smaller than the step variation. The conversion efficiency displays overshoot for the decrease cases and undershoot for the increase cases.

3) When load current is varied, the response of the output power is almost synchronous with the load current, however, the temperature distribution within the TEG and the corresponding heat adsorbed from the ambient can not response synchronously due to finite thermal diffusion rate, which causes not only the temporal hysteresis in the response of conversion efficiency to the load current, but also overshoot or undershoot of the conversion efficiency.

Acknowledgment

References

[1] D.M. Rowe, Thermoelectrics Handbook: Macro to Nano, CRC Press, BocaRaton, 2006.
[2] S.B. Riffat, X. Ma, Appl. Therm. Eng. 23 (2003) 913–935.
[3] F.J. Disalvo, Science 285 (1999) 703–706.
[4] B.J. Huang, C.J. Chin, C.L. Duang, Int. J. Refrig. 23 (2000) 208–218.
[5] K.H. Lee, O.J. Kim, Int. J. Heat Mass Transfer 50 (2007) 1982–1992.
[6] B.J. Huang, C.L. Duang, Int. J. Refrig. 23 (2000) 197–207.
[7] D.M. Rowe, M. Gao, J. Power Sources 73 (1998) 193–198.
[8] M. Chen, L.A. Rosendahl, T. Condra, Int. J. Heat Mass Transfer 54 (2011) 345–355.
[9] X. Gou, H. Xiao, S. Yang, Appl. Energy 87 (2010) 3131–3136.
[10] A.J. Minnich, M.S. Dresselhaus, Z.F. Ren, G. Chen, Energy Environ. Sci. 2 (2009) 466–479.
[11] H. Wei, Y.H. Su, S.B. Riffat, J.X. Hou, J. Ji, Appl. Energy 88 (2011) 5083–5089.
[12] J.G. Haidar, J.I. Ghojel, Waste Heat Recovery from the Exhaust of Low-power Diesel Engine Using Thermoelectric Generators, in: Proceedings ICT2001 20 International Conference on Thermoelectrics (2009), pp. 413–418.
[13] N. Espinosa, M. Lazard, L. Aixala, H. Scherrer, J. Electron. Mater. 39 (2010) 1446–1455.
[14] R.Y. Nuwayhid, D.M. Rowe, G. Min, Renewable Energy 28 (2003) 205–222.
[15] J. Yang, Potential Applications of Thermoelectric Waste Heat Recovery in the Automotive Industry, in: 24th International Conference on Thermo-electrics, 2005, pp. 170–174.
[16] C. Wu, Appl. Therm. Eng. 16 (1996) 63–69.
[17] R.Y. Nuwayhid, A. Shihadeh, N. Ghaddar, Energy Convers. Manage. 46 (2005) 1631–1643.
[18] G.W. Liang, J.M. Zhou, X.Z. Huang, Appl. Energy 88 (2011) 5193–5199.
[19] T. Kousksou, J.P. Bedecarrats, D. Chmpier, P. Pignolet, C. Brillet, J. Power Sources 196 (2011) 4026–4032.
[20] W. Sun, P. Hu, Z.S. Chen, L. Jia, Energy Convers. Manage. 46 (2005) 789–796.
[21] M. Chen, L.A. Rosendahl, I. Bach, T. Condra, J.K. Pedersen, Transient Behavior Study of Thermoelectric Generators Through an Electro-thermal Model Using Spice, in: International Conference on Thermoelectrics, 2006.
[22] A. Montecucco, J.R. Buckle, A.R. Knox, Appl. Therm. Eng. 35 (2012) 177–184.
[23] M. Alata, M.A. Al-Nimr, M. Naji, Int. J. Thermophys. 24 (2003) 1753–1768.
[24] X.D. Wang, Y.X. Huang, C.H. Cheng, D.T.W. Lin, C.H. Kang, Energy 47 (2012) 488–497.
[25] J.H. Meng, X.D. Wang, X.X. Zhang, Appl. Energy 108 (2013) 340–348.
[26] C.H. Cheng, S.Y. Huang, Appl. Energy 100 (2012) 326–335.
[27] D.M. Rowe, Renewable Energy 16 (1999) 1251–1256.
[28] B. Jang, S. Han, J.Y. Kim, Microelectron. Eng. 88 (2011) 775–778.
[29] S.W. Angrist, Direct Energy Conversion, third ed., Allyn and Bacon, 1976, pp. 140–166.